Computers and Electronics in Agriculture 145 (2018) 217–225

Contents lists available at ScienceDirect

Computers and Electronics in Agriculture

journal homepage: www.elsevier.com/locate/compag

Original papers

Mapping forests using an unmanned ground vehicle with 3D LiDAR and graph-SLAM

Marek Pierzchała[a,*], Philippe Giguère[b], Rasmus Astrup[a]

[a] Norwegian Institute of Bioeconomy Research, PO Box 115, 1430 Aas, Norway
[b] Department of Computer Science and Software Engineering, Laval University, Quèbec, Canada

ARTICLE INFO

Keywords:
SLAM
LiDAR
Forest operations
Precision forestry
DBH

ABSTRACT

Enabling automated 3D mapping in forests is an important component of the future development of forest technology, and has been garnering interest in the scientific community, as can be seen from the many recent publications. Accordingly, the authors of the present paper propose the use of a Simultaneous Localisation and Mapping algorithm, called graph-SLAM, to generate local maps of forests. In their study, the 3D data required for the mapping process were collected using a custom-made, mobile platform equipped with a number of sensors, including Velodyne VLP-16 LiDAR, a stereo camera, an IMU, and a GPS. The 3D map was generated solely from laser scans, first by relying on laser odometry and then by improving it with robust graph optimisation after loop closures, which is the core of the graph-SLAM algorithm. The resulting map, in the form of a 3D point cloud, was then evaluated in terms of its accuracy and precision. Specifically, the accuracy of the fitted diameter at breast height (DBH) and the relative distance between the trees were evaluated. The results show that the DBH estimates using the Pratt circle fit method could enable a mean estimation error of approximately 2 cm (7–12%) and an *RMSE* of 2.38 cm (9%), whereas for tree positioning accuracy, the mean error was 0.0476 m. The authors conclude that robust SLAM algorithms can support the development of forestry by providing cost-effective and acceptable quality methods for forest mapping. Moreover, such maps open up the possibility for precision localisation for forestry vehicles.

1. Introduction

Over the last two decades, technological developments in remote sensing and computing capabilities have altered the way information about forests is collected and processed. In Fennoscandia, airborne laser scanning (ALS), also known as LiDAR scanning, has been the main approach to developing estate-level forest inventories for over a decade (Næsset et al., 2004). Given improved sensors and improved image processing algorithms, both automatically generated photogrammetric point clouds obtained from aircraft (White et al., 2013; Rahlf et al., 2015) and unmanned aerial vehicles (UAVs) (Pierzchała et al., 2014; Puliti et al., 2015) are rapidly gaining widespread use and popularity in forestry. In general, image processing is carried out offline, either using robust computer vision algorithms to obtain highly precise and accurate 3D representation of surfaces, or using orthomosaics that are suitable for mapping (Turner et al., 2012). Additionally, ground-based sensors, especially terrestrial laser scanning (TLS), have received significant attention with respect to forest inventories (Liang et al., 2016) over the past decade. TLS has been used to obtain measurements of a wide array of forest attributes, including classic inventory variables (Liang et al., 2016), root systems (Smith et al., 2014), canopy and leaf attributes (Béland et al., 2011; Ducey et al., 2013), and wildlife habitats (Olsoy et al., 2014). In many cases, TLS has been shown to measure key variables such as stem diameter and volume with high accuracy (Liang et al., 2016) but in some cases there has been poor correlation between the TLS measurements and observed tree diameters (Ducey et al., 2013). Although ALS and photogrammetry are gaining widespread operational use, the application of TLS in forestry is still more popular in much of the research community than in operational management and inventorying. For operational use, TLS faces a number of challenges: is time and labour-intensive to carry, mount, and collect the data in the forest; it is both time and computationally demanding to process the data in the office; and there are significant challenges with non-detection of trees if multiple scans are not performed and stitched together (Astrup et al., 2014; Liang et al., 2016). Various promising attempts have been made to overcome these challenges, including correction for non-detection in single scans (Astrup et al., 2014), automatic stitching of multiple scans into a single point cloud (Liu et al.,

* Corresponding author.
E-mail address: Marek.Pierzchala@nibio.no (M. Pierzchała).

https://doi.org/10.1016/j.compag.2017.12.034
Received 2 February 2017; Received in revised form 20 December 2017; Accepted 24 December 2017
Available online 08 January 2018

2017), and the use of TLS as a ground-truth for ALS applications (Hauglin et al., 2014). An alternative to traditional TLS applications is mobile laser scanning (MLS). MLS holds significant promise in forestry (Holopainen et al., 2014) but its application is still immature and only a few studies of MLS in forests have been conducted (Miettinen et al., 2007; Tang et al., 2015; Jaakkola et al., 2010; Rönnholm et al., 2016). MLS in forest environments faces a number of challenges, foremost among which is locating the position and movement of the scanner, given poor global navigation satellite system (GNSS) coverage under the canopy. Precise localisation under a forest canopy is a complex problem but, if the problem can be resolved, the method can open up numerous opportunities in forestry. For example, knowledge of the position of a forest harvester can allow for the precise geolocation of harvested trees. Another advantage of precise localisation is the ability to perform autonomous navigation in a forest (Hellström et al., 2006). One potential solution to the problem of localisation in forests is the use of simultaneous localisation and mapping (SLAM) algorithms (Siciliano and Khatib, 2008), which have been developed in the mobile robotics community.

Mapping and localisation are important components of advanced autonomous navigation systems for mobile robots. A map is required in order to perform any type of path planning algorithms, in order for a robot to navigate to its goal position. Maps are also required for localisation, with the latter usually defined with respect to the generated map frame of reference (as opposed to a global reference, such as with GNSS). The SLAM paradigm rests on Bayes filtering, a well-known probabilistic inference approach that tries to fuse different sources of information (odometry, measurements, and motion commands) in an optimal or near-optimal manner. Most importantly, the approach takes into account the various uncertainties (noise) from every source. A common type of sensor used to obtain such measurements is a camera. These rich sensors allow the extraction of robust natural visual landmarks, and the creation of maps consisting of their localisation (either within a single global frame of reference or with multiple frames of references). Computer vision algorithms, such as the Oriented FAST and Rotated BRIEF (ORB) descriptor, have been used to perform both landmark extraction and matching, culminating in the popular ORB-SLAM algorithm (Mur-Artal et al., 2015). However, vision algorithms suffer greatly from the fact that they require a strong matching of these visual landmarks between pose and have limited depth precision (for stereo) or none (for monocular systems, as they find geometry up to a scale factor). By contrast, range sensors such as LiDAR typically have good depth perception, and the newer models having somewhat higher bandwidths (over half a million points per second). They allow the creation of dense map representations, both in 2D and 3D; in other words, no landmarks are extracted, but rather most of the data are stored in the map. Such maps can be multilevel surface maps (Triebel et al., 2006), point clouds, and occupancy grids (Wurm et al., 2010). Dense maps are interesting not only for robot navigation but also because they provide more information about the environment, which makes it attractive to use them a posteriori. In the context of mapping forests, a prominent example is the use of such dense 3D maps for inventory purposes.

The use of SLAM has been explored previously in forest environments using 2D LiDAR combined with GPS (Miettinen et al., 2007) as well as small footprint LiDAR, IMU, and GPS for 2D SLAM (Tang et al., 2015). The goal of this paper was to test graph-SLAM for mapping of a forested environment using a 3D LiDAR-equipped UGV. The first sub-goal was to test the feasibility of creating a 3D point cloud representing the ground surface and lower stems based on data captured by the UGV. The second sub-goal was to quantify the accuracy of the extracted diameters and distances between stems together with development of support ratio as a function for determining the fraction of stem that is covered with laser points.

2. Theoretical background

In this section, we describe theoretical background of the SLAM paradigm, particularly the graph-SLAM concept. This includes the importance of its components such as odometry, loop closure and graph optimisation. We then present an overview of the technical aspects of our test, including the mapping platform and its elements as well as the field area used for testing. Thereafter, we describe the software architecture and process of map creation. We conclude by specifying the methods for data extraction which are used for quantifying the accuracy of our approach.

2.1. The SLAM concept

Generally speaking, the SLAM problem (in its full-SLAM variant) lies in estimating the posterior probability of the robot's complete trajectory $x_{1:T}$ and the map $\mathbf{m}$ of the traversed environment, given all the measurements $z_{1:T}$ and motion commands $u_{1:T}$, plus an initial position x_0 (Grisetti et al., 2010):

$$p(x_{1:T},\mathbf{m}|z_{1:T},u_{1:T},x_0). \quad (1)$$

For wheeled vehicles, wheel odometry is often used to compute a priori pose estimates in lieu of the true command u, before being corrected by exteroceptive sensor measurements z. However, due to the high probability of wheel slippage in forested environments (Ringdahl et al., 2012), several alternative strategies to pure odometry have been proposed. For instance, Nister has reported an extensive study of field testing of visual odometry in ground vehicle applications (Nistér et al., 2006).

2.1.1. Graph-SLAM approach

A number of SLAM solutions have been proposed. Earlier ones were based on Extended Kalman Filters (Bailey et al., 2006), where the state estimation included the map $\mathbf{m}$ of the position of all n landmarks. Due to the inherent computational complexity of $O(n^2)$ for these Kalman-based solutions, graph-SLAM approaches have reformulated the SLAM problem as a graph-related problem. In these approaches, a node represents a particular robot pose x_t, while edges encode either odometry or loop-closure constraints. For either edge, they represent a transformation matrix (rotation and translation) along with a covariance matrix encoding the uncertainties associated with these transformations. Once a graph representing the SLAM problem has been created, a global relaxation algorithm is used to optimise the trajectory $x_{1:T}$, in order to minimise the non-linear odometry and loop closure constraints and thus find the most likely map $\mathbf{m}$. Importantly, loop closures explicitly allow the correction of the accumulated errors during displacements. After optimisation, corrections are back-propagated along these loops, thus improving the map. An example of this effect on scan reassembly is shown in Fig. 1.

3. Material and methods

3.1. Hardware and software setup

To carry out the field tests, we built a dedicated mobile platform on top of a standard 4 wheeled rover 'Superdroid 4WD IG52 DB' (Fig. 3), which was controlled via a Spektrum DX5e remote controller for driving of the vehicle in the forest. An aluminium frame bolted on top of the Superdroid was used to carry the various sensors. At the highest point of the frame was our main sensor for mapping, a Velodyne VLP-16 LiDAR, used for acquisition of the 3D point clouds. The VLP-16 is a compact 3D scanner with 16 laser/detector pairs with a 360° horizontal field of view and a 30° vertical field of view. The laser beams have a divergence of 3 mrad. Full 360° scans of 300,000 points are acquired with frequencies of 2 Hz. According to the vendor manual, the scanner operates with a normal accuracy of ± 3 cm. The maximum range of the

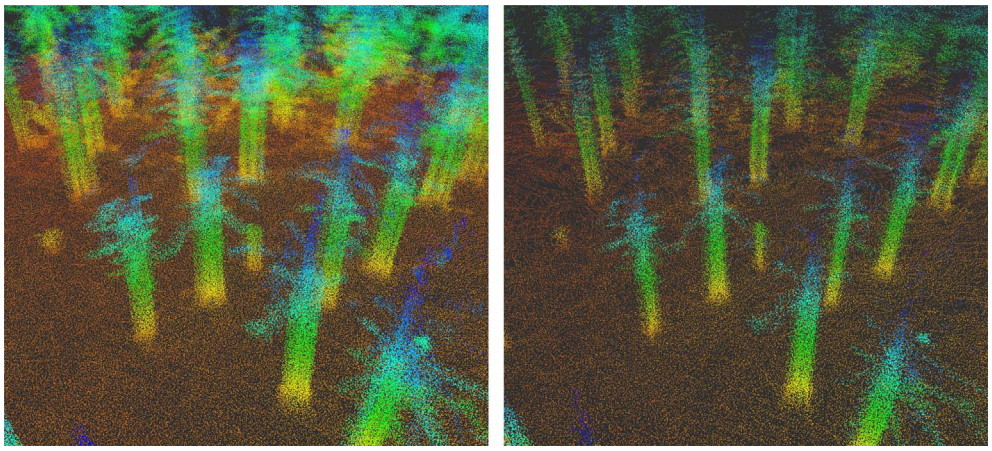

Fig. 1. The assembled stem map before (left) and after (right) loop closure detection and graph optimisation. The map on the right shows a reduction of scan misalignment.

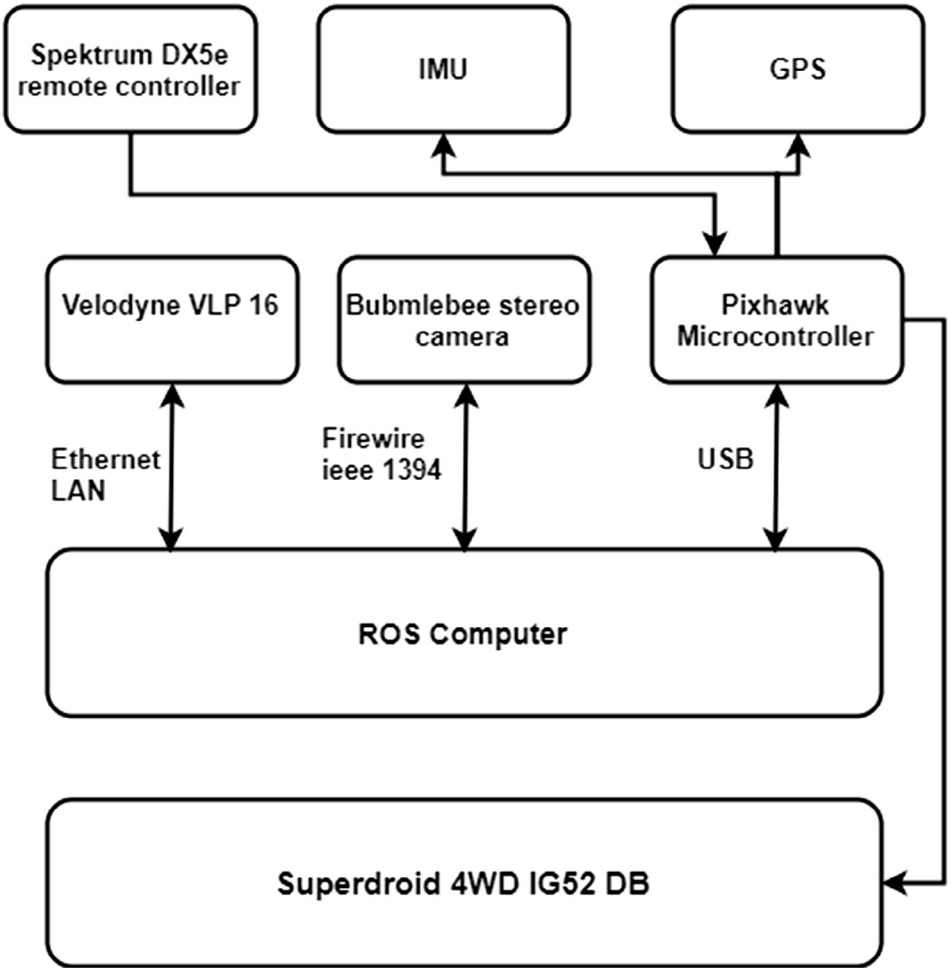

Fig. 2. System scheme showing the elemtents of our setup.

VLP-16 is up to 100 m, depending on the reflectivity of the target surface. Secondary sensors for collecting complimentary data included a Bumblebee® stereo vision camera (by Point-Grey) to record stereo images. A Pixhawk Microcontroller was used as a sensor and device bridge, passing command messages from the RC controller, and providing information from its integrated IMU and GPS, for global reference. The system scheme is presented in Fig. 2.

For software infrastructure, we employed the Robot Operation System (ROS) (Quigley et al., 2009), Indigo Igloo, run on Ubuntu 14.04 LTS. This software allows for real-time processing and offers data collection mechanisms that allow for offline processing. It offers a standardised publish/subscribe architecture, along with drivers for all of our sensors. It also provides a time-stamp for every piece of information collected. A standard laptop PC was used as the ROS master, which manages all software components (called nodes) that share tasks and run ROS on other machines, via standard IP protocol.

3.2. Test area, robot path selection and data capture

The field test was carried out in southern Norway, c. 30 km south of Oslo. A mature pure Norway spruce stand of relatively high productivity was selected for mapping. Table 1 summarizes the stand

Fig. 3. The mobile platform used for data collection purposes, based on the 'Superdroid 4WD IG52 DB' rover. The grey and black cylinder at top right is the VLP-16 LiDAR. The golden rectangular device at top left is the Bumblebee stereo vision camera.

Table 1
Table that summarizes the stand selected for testing. The age of the forest is approximately 60 years.

Key features	Value
Number of trees (ha)	961
Max height (m)	27
Mean height (m)	25.4
Mean DBH (cm)	25.7
Basal area (m^2/ha)	49.8
Volume (m^3/ha with bark)	643.8

properties. The terrain was relatively flat, with low amounts of understory vegetation allowing for relatively easy manoeuvring of the mobile platform.

During data collection, the robot was driven through the stand, which covered an area of c. 900 m^2. The total distance driven was 130.7 m with an average speed of 1 m/s. The route was chosen to cover most of the area and at the same time allowing for maneuverability between the trees. The robot path included three loops within the test area. As mentioned in Section 2.1.1, SLAM algorithms require that loops are present in the trajectory in order to cap uncertainty and back-propagate errors upon loop-closure detection. Loop closure constraint requires only 2 loops and the graph was optimized right after a second loop was initiated. The third loop was intended for densyfying the dataset.

3.3. Point cloud creation

The automatic map creation is based on the standard 3D graph-SLAM algorithm GTSAM (Dellaert, 2012). The non-linear graph optimisation problem is solved using the Levenberg-Marquardt method, as presented in Dellaert (2012). This step is referred to as the SLAM back-end. This problem is solved by seeking the configuration of nodes that maximizes the likelihood of the observations encoded in the constraints (Grisetti et al., 2009).

In many cases, SLAM can be used in a context of real-time map creation and localisation. However, for our research, map quality was prioritized over real-time mapping and the maps were created with offline post-processing. This is justified by our goal of evaluating the map as a product of SLAM workflow. Real time mapping is important, but we do not discuss the benefits and shortcomings of this aspect in this paper. In order to perform the offline map construction within the ROS architecture, we played and processed the recorded data from the field at half the speed of the actual data capture using the same hardware resources. The reduced speed ensured that all information (broadcasted messages) was fully processed and not dropped due to overruns. 3D point clouds with a full 360° field of view were generated, with a maximum range of 12 m and vertical field of view of 30°. The graph was built solely from laser odometry (O) which was estimated using the Iterative Closest Point (ICP) algorithm (Nelson, 2016). Wheel odometry was not used because the rover did not have wheel encoders. Nevertheless, it is generally assumed that wheel odometry in forests is unreliable, due to rough terrain and frequent wheel slippage. The ICP parameters were set as follows:

- maximum number of iteration is 2000
- convergence is assumed if the transformation from the last iteration was less than 10^{-10}
- corresponding points with a distance greater than 0.5 m are ignored
- transformation thresholding was not applied (although limiting the search space for scan alignment can speed up the process for real-time operations).

Loop closure is a critical component of any graph-SLAM approach, and must therefore be carefully parametrised. We empirically selected a number of parameters, the most important ones being:

- translation threshold of 0.5 m, which is the minimum distance needed to cast a new pose to the graph
- proximity threshold 1.5 m, which defines the search space for old poses, and thus relates to the quality of the odometry
- Loops were not closed within the 10 most recent poses
- the number of poses before reclosing is 10.

After each loop closure and optimisation step, a map was constructed as an octree-based decimation with a leaf size of 0.01 m. The result was exported at the end of mapping process as a text file, which comprised "point triplets" representing the 3D point coordinates.

3.4. Extraction of stem diameters and positions from the SLAM map

Based on a series of existing algorithms we developed a procedure to automatically extract the diameter breast height (DBH) of each tree in our 3D point cloud. First, all the points representing the ground were identified using a standard plane fitting approach based on random sample consensus (RANSAC) (Schnabel et al., 2007). After the ground points had been identified, a ground surface mesh was generated by applying a Poisson surface reconstruction (Kazhdan and Hoppe, 2013) with the octree method, where the octree level was arbitrarily set at a value of 5. Second, the signed distance (SD) between the ground surface and all non-ground points was computed as a normalization procedure. We chose a normalized height value in the range 1.2–1.4 m, as this represented the standard measurement height of DBH. These labelled points were then projected onto a plane, such that 2D analysis could be applied.

In the 2D point map, we identified individual tree stems using density-based spatial clustering of applications with noise (DBSCAN) (Ester et al., 1996). The two parameters used in this method were (i) the minimum number of points supporting the cluster and (ii) the maximum point to point distance within the cluster. In our test, we choose the value of $i = 0.3$ m and $ii = 15$ cm, respectively. This resulted in 2D positions of cluster centroids, their numbers, and the indexes of points belonging to each cluster. For each cluster, a circle was fit under the assumption of a circular cross-section. Two different circle-fitting approaches were employed. The first approach was based on minimising the root mean square error (RMSE) of the fitted circle. The second approach was the direct application of the method proposed by Pratt (Pratt, 1987). The two methods were applied together with RANSAC in order to improve the fitting and to obtain the number of inliers. The RANSAC parameters were:

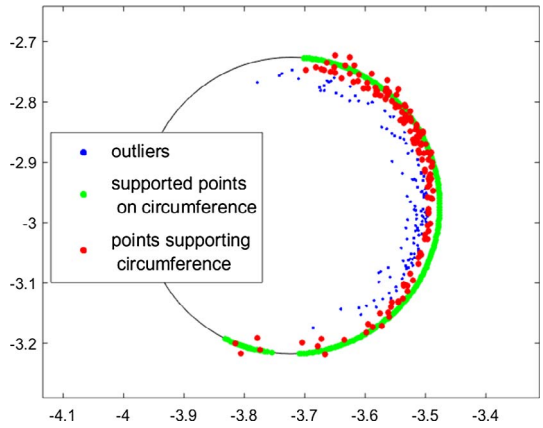

Fig. 4. Visualisation of the support ratio *S*. On the fitted circle, the green points indicate the proportion of stem circumference that is supported by inliers (red points). The outliers (blue points) were not used for estimation of the support ratio. The small gap between green points on the lower edge of the circle is due to the fact that there were no laser points within the specified error value $\epsilon = 2$ cm. (For interpretation of the references to colour in this figure legend, the reader is referred to the web version of this article.)

- number of RANSAC trials: $n_{tr} = 100$
- error value: $\epsilon = 0.02$ m.

These two methods returned individual metrics representing DBH, which we named D_{ls} for the least squares method and D_{Pratt} for the Pratt method. The positions of single trees were obtained from coordinates of circle centres that were fitted against each cluster.

Some of the trees did not have full point coverage around their stems. We attribute this to the fact that the trajectory of the rover did not allow for a full 360° view of the tree. We devised a simple metric, which we named *Support ratio S*, to gain a better understanding of how the point coverage of individual trees affected the accuracy of their estimated DBH. To compute the metric *S*, we placed 360 equally spaced points on the circumference of the fitted stem circle. For each point on the fitted circle, a linear distance to all points in the cluster was computed. Points outside of the mentioned error value ϵ were not used to calculate the support ratio. The procedure for calculating the support ratio is presented in Algorithm 1. The support ratio *S* can be visualised as the proportion of points laying on the fitted circle, as depicted in Fig. 4.

Algorithm 1. for calculation of support ratio *S*

1: Reconstruct the stem circle (x_{fit},y_{fit},R_{fit});
2: Give the minimum support to circumference ϵ;
3: Compute *x*,*y* positions of points on reconstructed circumference at every 1° interval;
4: **for** each point on reconstructed circle; **do**
5: **for** each point in cluster; **do**
6: compute linear distance;
7: **end for**
8: find minimum distance d_{min};
9: **if** $d_{min} \leqslant \epsilon$, **then**
10: select the point;
11: **else**
12: do not select the point;
13: **end if**
14: **end for**
15: sum all selected points;
16: Compute the ratio *S* by dividing all selected points by the count of all points on reconstructed circle;
17: **return** *S*

3.5. Evaluation of the accuracy of extracted diameters and stem positions

We evaluated the extracted stem positions and diameters against data that were obtained by manual measurements of trees in the plot. For each stem, two measurements at breast height were taken using a calliper. The mean of these two measurements was the DBH value used as ground truth.

Since it proved too difficult to find the absolute position of trees in the stand, we used the relative distance between trees. We therefore selected six trees that were distributed uniformly over the mapped area and then measured the horizontal distance from each of the selected trees to all trees in the line of sight that were included in research plot. Distance measurements were taken using a Leica Disto D3A Laser Rangefinder. Single measurements were taken by placing the instrument against the stem surface of tree A and directing it towards tree B, with the tangent point as the zero point. To obtain the distance between the tree centres, we added the values of the radiuses of trees A (r_A) and B (r_B) to the measured horizontal distance ($l_{(A,B)}$). The corresponding distance on the map was obtained from point coordinates (*A*,*B*). The error for distance estimation E_{dist} was calculated with Eq. (2):

$$E_{dist} = l_{(A,B)} + r_A + r_B - \sqrt{(A_1 - B_1)^2 + (A_2 - B_2)^2}. \quad (2)$$

The accuracy of the methods was evaluated with respect to the mean error of estimate (otherwise termed mean signed deviation MSD to indicate bias) and the root mean square error (RMSE). All statistical computations were performed in Matlab®.

4. Results

We built the 3D map of the plot based on the data collected by our robot, which was driven over a total distance of 130.7 m, with 2 large loops and one small loop. During this trajectory, 14 loop closures were detected. Fig. 5 shows the reconstructed point cloud at the end of mapping process when all loops were closed, and Fig. 6 shows the lower stems visualised as simple cylinders. Figs. 5 and 6 also show the robot's trajectory.

We applied our automatic tree extraction procedure to the built 3D point cloud. In total, we found 78 clusters, of which 71 constituted trees and 7 constituted other objects, such as understory vegetation without visible stems. The large number of clusters was due to the appropriate choice of parameters for the DBSCAN clustering algorithm. For every tree that was found, we estimated two DBH values (D_{ls} and D_{Pratt}) for the respective method. Fig. 7 shows eight examples of clusters with their estimated support ratio and fitted DBH.

A comparison between the estimated and manually measured diameters is shown in Fig. 8 (left-hand graph). The average diameter was 24.7 cm. The mean estimation errors are listed in Table 2, which shows how many trees were present in different support ratio classes and that significant outliers were associated with a low proportion of support ratio *S*. From Fig. 8 (left), it can be seen that many values were overestimated. The corresponding mean errors in Table 2 shows that modelled DBH values were overestimated up to the support value $S = 0.6$ for D_{Pratt} and D_{ls} and underestimated above this value to a maximum of 20%. There were too few observations to show any eventual dependency of the errors on DBH class.

We also tried to determine the impact of the support ratio *S* on the estimation of the DBH for a fixed ϵ value of 2 cm. As the support ratio *S* decreased, we expected reduced estimation accuracy. Values for all 71 clusters representing stems are plotted in (Fig. 10). Fig. 10 shows how the error in DBH estimation decreases with the increasing support ratio *S* up to a $S = 0.65$ where the bias (MSD) approaches 0. Past $S = 0.65$ the bias becomes negative and resulting *RMSE* increases. In addition, we analysed how varying the error value ϵ influenced the number of trees in the respective support ratio classes (Fig. 9). Fig. 9 shows how decreasing the value of ϵ lowers the support ratio *S*. High values of ϵ result

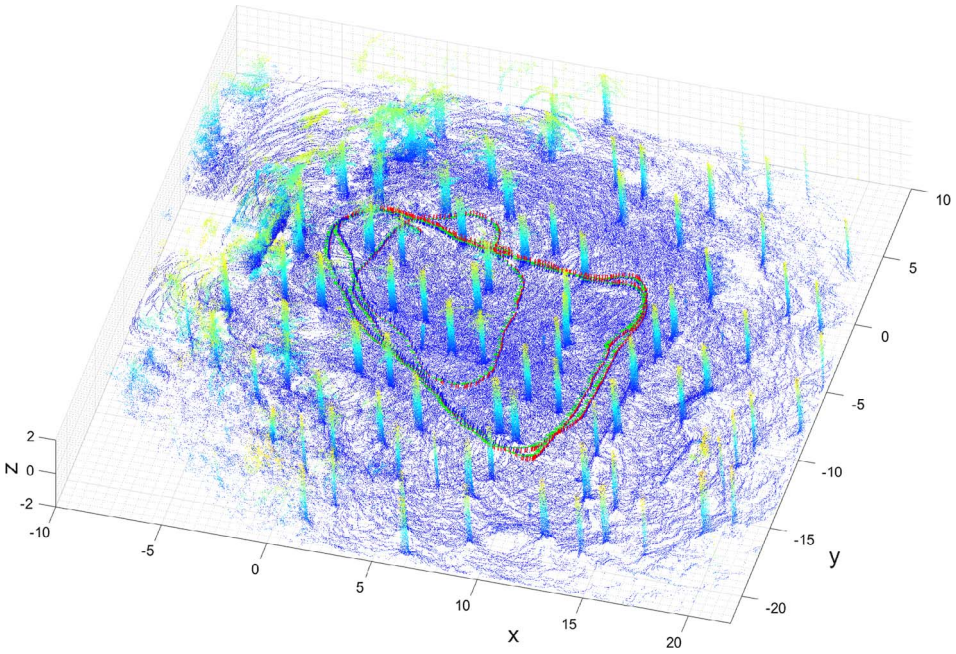

Fig. 5. The reconstructed point cloud for the ground surface and lower stems and the robot trajectory with its 3 loops.

in erroneous inclusions of points (laser measurement "noise") leading to an overestimation of S. In our data the number of trees for the respective threshold values of S was lower for small values of ϵ.

In the second part of evaluation we have assessed the path with use of relative distances between the trees. The distances obtained from laser measurements taken in the field resulted in 278 single measurements (from tree indexes 4,17,32,45,63, and 69). The modelled- and manually measured distances are compared in Fig. 8 (right-hand graph). Overall, the trees' relative positions extracted from our SLAM map were very accurate. However, four outliers were clearly visible, which we suspect arose from incorrect tree labelling in the field. When these outliers were removed, the mean error value for modelled distance measurement was $\overline{E}_{dist} = 0.0476$ m.

5. Discussion

Mobile mapping in forests is a relatively new field of research and our results are promising. Our developed hardware setup in combination with the applied software configuration and algorithms proved successful in terms of producing an internally consistent map of the forest environment.

The selected study area was easy to access and there was no understory, which is a quite uncommon condition in many forested environments. The structural characteristics of the surrounding environment had an impact on the performance of SLAM. In contrast to other environments, such as cities or buildings, forests are not well structured and their environmental conditions vary greatly with seasonal changes. Fine elements such as branches, small trees, and leaves are generally difficult to capture with the available sensor resolutions, and thus might present a challenge for mobile mapping. Another challenge is occlusion

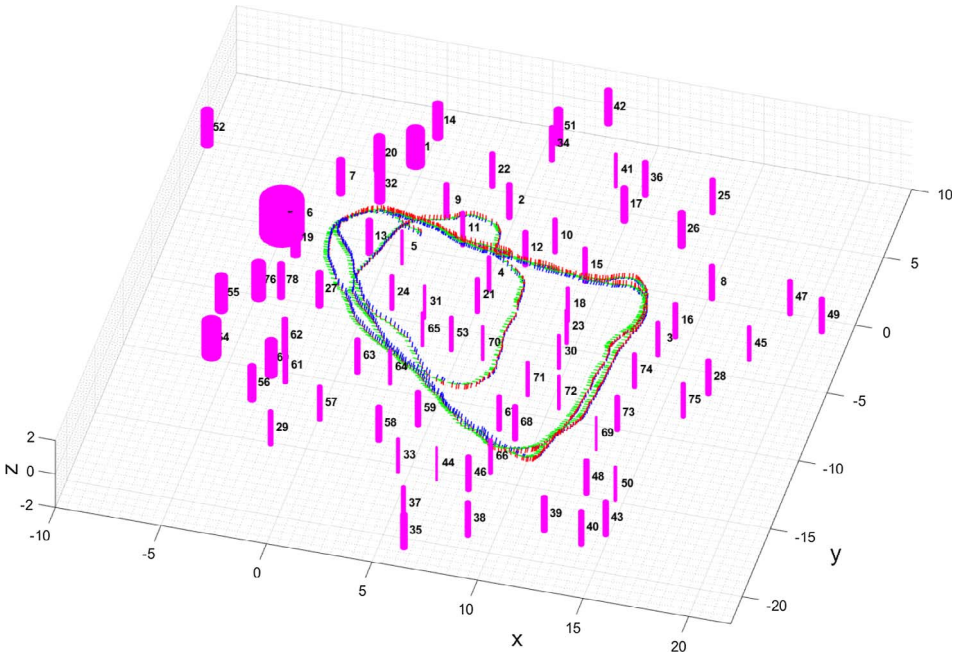

Fig. 6. Stem cylinder map based on their circle-fitted DBH and the robot trajectory with its 3 loops.

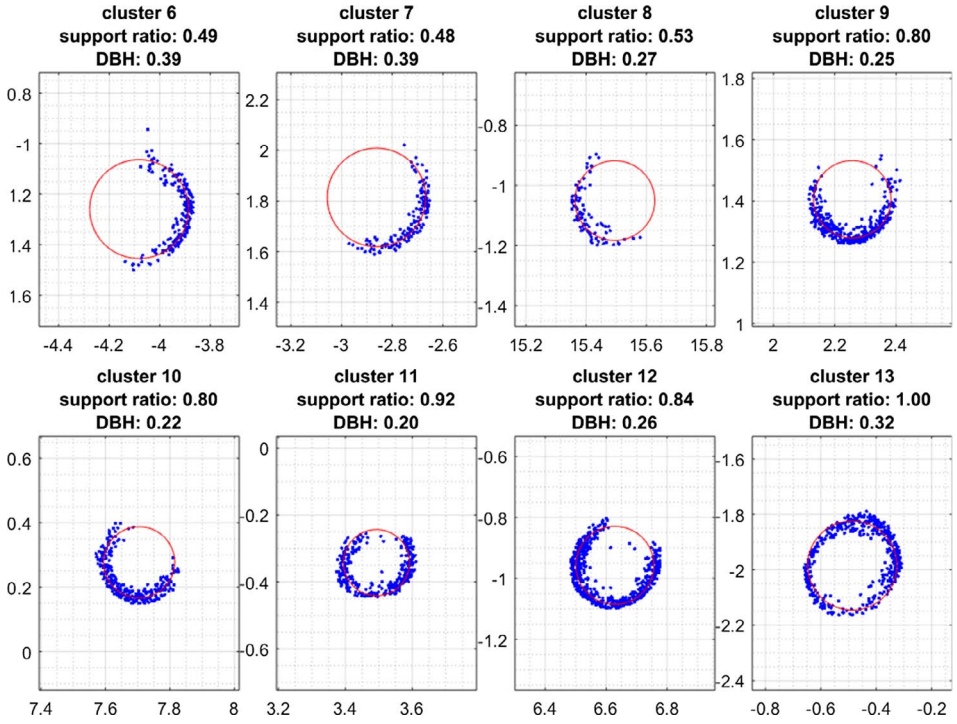

Fig. 7. Eight examples of 2D point clusters and their fitted stem circle at breast height with their respective diameters (m) and support ratios *S*.

from branches and low vegetation. The absence of large continuous surfaces such as tree trunks can reduce the quality of the laser odometry, due to the need in the ICP algorithm to perform nearest-neighbours assignments that correspond to the same physical surface. In our test we believe that scan matching performed well due to a relatively clear view and branch-free lower stems in much of the study area. Nevertheless, more tests should be conducted to gain a better understanding of the possibly detrimental effect of for example ground vegetation on mapping success. In our study, we artificially capped the range of the sensor to 12 m, in order to secure a sufficient number of ground points, which were essential for scan matching during the ICP procedure. When testing with a shorter range (not discussed in the Results section), and with fewer ground points obtained, the scan matching was generally not successful, indicating that the tree trunks alone cannot be used for alignment. With increasing range, the farthest points were sparse and suffered from abrupt occlusions by the nearest trees, which in both cases is detrimental to the performance of the ICP algorithm. In this context, finding an optimal range for a LiDAR sensor is an important consideration and an interesting direction for future research.

In forestry most of the studies with terrestrial capture pointclouds have relied on high quality expensive scanners and known scanner positions (Liang et al., 2016; Liu et al., 2017). The point cloud generated in this study is fundamentally different due to different type of LiDAR scanner and different positioning method. In our case we relied on point clouds preprocessed by the mapping algorithm and re-sampled after loop closure. It should also be noted that the LiDAR sensor used in our study is not optimised for 3D reconstruction but rather for mapping purposes. Finally, we did not correct for the sensor displacement during each revolution of the scanner (0.1 s).

The map validation in terms of tree positioning returned good results compared with the results of previous studies. For example, Tang et al. (2015) reported errors on the trajectory when using a SLAM algorithm based on improved maximum likelihood estimation (IMLE) supported with IMU. These errors were 0.32 m, and 2.90 m (*RMSE*) depending on the area, but no information on tree positioning accuracy was given. Miettinen et al. (2007) used a combined SLAM approach for forest mapping, but did not report mapping accuracy because the manually measured map was too inaccurate with respect to the position of the individual trees. In the study conducted by Forsman et al. (2016),

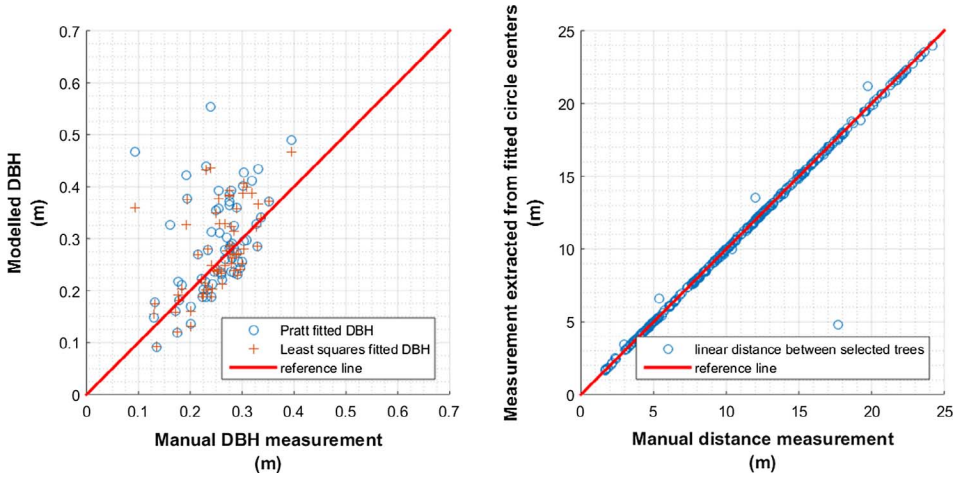

Fig. 8. A comparison of modelled and manual measurements for DBH and stem distances. The left-hand graph shows the relationship between DBH extracted from the fitted circles and DBH measured with a calliper. The right-hand graph shows the relationship between linear distances obtained from modelled circle centres and distances measured with a hand-held laser.

Table 2
Mean errors of estimate and root mean squared errors for modelled DBH for varying support ratios, according to the two different circle-fitting methods (D_{Pratt} and D_{ls}).

Support ratio class S	D_{Pratt} trees in class	D_{Pratt} mean error (cm)	D_{Pratt} mean error (%)	D_{Pratt} RMSE (cm)	D_{Pratt} RMSE (%)	D_{ls} trees in class	D_{ls} mean error (cm)	D_{ls} mean error (%)	D_{ls} RMSE (cm)	D_{ls} RMSE (%)
0.1	1	60.88	338.25	60.88	338.25	1	87.65	486.95	87.65	486.95
0.2	5	23.2	141.2	25.56	163.65	4	23.0	163.91	24.09	193.8
0.3	9	15.75	133.5	29.57	323.45	10	15.36	119.67	26.52	280.98
0.4	10	5.77	22.94	8.78	35.5	9	6.48	26.27	8.71	35.5
0.5	12	4.97	18.34	6.45	23.02	13	4.90	17.93	7.4	26.19
0.6	6	2.2	12.0	2.38	8.51	7	0.01	1.26	2.82	10.02
0.7	3	−1.92	−7.35	2.50	9.1	3	−3.07	−12.65	3.53	13.63
0.8	12	−2.39	−9.19	2.94	11.34	12	−2.63	−10.27	3.21	12.66
0.9	4	−3.83	−15.94	3.95	16.48	3	−3.28	−13.64	3.29	13.68
1	8	−4.12	−20.1	4.64	23.05	8	−4.31	−20.73	4.81	23.36

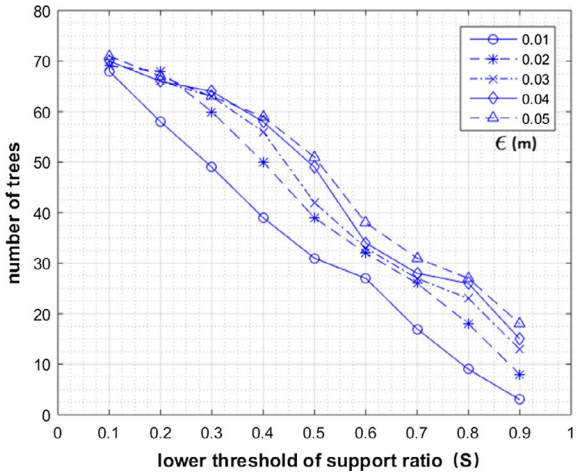

Fig. 9. The available numbers of trees (*y*-axis) with different threshold values of support ratio (*x*-axis) for varying values of ϵ (in the legend). For example, given a minimum support ratio of 0.5 the available number of trees varies between 30 and 50, depending on the chosen error value ϵ.

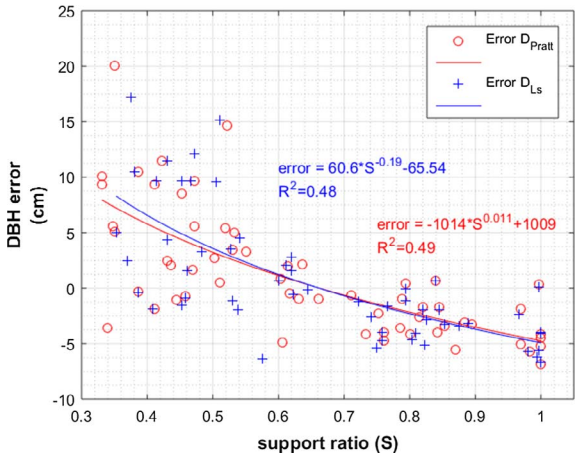

Fig. 10. The relationship between the relevant support ratios and respective errors of estimate for modelled DBH. The *x*-axis represents the proportion of fitted circle circumference supported by laser points (S). The *y*-axis shows the error between modelled versus measured diameter.

the mapping was affected by position drift and the authors concluded that there was a need to implement their stem detection method in combination with a SLAM algorithm.

The comparison between the stem extraction approaches and the diameters measured in the field shows that the different approaches yielded diverging results. In our study, we extracted DBH by means of circle fitting on 2D data set subtracted from a 3D data set. The advantage of this approach is that it is fast and easily implemented to obtain the 2D representation of tree diameters by projecting points, filtered by a signed distance that corresponds to diameter at breast height. The lack of understory and relatively flat terrain in our study site made ground segmentation relatively easy and allowed for successful plane fitting. However, in complex terrains, methods that are more sophisticated might be required, including knowledge of the map orientation (Vosselman and Maas, 2010). Finding trees by means of density-based clustering was successful in this study, but this process is computationally expensive. The methods for obtaining diameters showed differences on the fitted circles (Fig. 8 and Table 2).

From the literature, it is clear that deriving DBH from mobile scanning data is not an easy task. Forsman et al. (2016) proposes methods for DBH modelling from LiDAR 2D scans and reports similar results to those presented here, in terms of precision and, given similarly sized trees. The best results from Forsman's study (Forsman et al., 2016) were 2.3% (6 mm) and *RMSE* of 14% (37 mm). Brunner and Gizachew (2014) applied a trigonometric approach to tree extraction and reported a bias of 3.7 cm and an RMSE of 6.8 cm.

In contrast to previous studies, we investigated the impact of the support ratio on DBH measurements. The support ratio *S* represents the fraction of the tree circumference that was scanned. This type of fraction of support points on tree modelling is also mentioned in Thies' work on evaluating TLS (Thies and Spiecker, 2004). Without giving explicit numbers for support ratio, they showed clearly that multiple scans improved the measurements. Our own results showed that the diameter estimation improved with increasing support ratios (Fig. 10) and for trees with a support ratio of 0.6, our results showed a D_{Pratt} mean error of −2.2 cm (−12%) and an *RMSE* 2.38 cm, and a D_{ls} mean error of −0.01 cm (−1.2%) and an *RMSE* of 2.82 cm. In Ringdahl et al. (2013) the circle fit method overestimated the diameter by 40%. Our results would indicate that this could be the result of the relatively low support ratio enabled by his methods. Ringdahl's use of enhanced algorithms and compensating for laser beam width reduced this error to less than 12%, slightly above our minimum error of −7.35% and 1.25% for g D_{Pratt} and D_{ls}, respectively (Table 2). It is important to mention that the support ratio *S* is derived from circle fit methods, which means that its value does not reflect the real support that in reality should be seen around half of the stem. Therefore, a support ratio below the value of 0.4 might indicate either bad quality of the fitting method or bad quality of the tree scan. Compared to TLS studies, in which good correlation between single scans and/or multiple scans and diameters have been frequently observed (Liang et al., 2016), mobile mapping studies are still in their infancy. Moreover, the sensors employed in mobile mapping, such as our mapping, are of much lower resolution, and simultaneously have to deal with the localisation challenge, both of which potentially contribute to decreased precision.

Finally, it is important to note that the mobile platform utilised in our study was not explicitly designed to be operational in a forest. Rather, it was developed for the investigation of mapping forest environments, with a focus on sensor performance and computer

algorithms. The question of robot's mobility in forested environments is a separate consideration that deserves attention, with some initial studies carried out in the context of 3D mapping such as the one by Arita et al. (2016).

6. Conclusions

In this paper, we have reported a successful implementation of graph-SLAM in a forest environment. The proposed method generated a map that was evaluated for its suitability to deliver stand properties such as DBH and coordinates for the positions of single trees. Together with the map, a graph that describes the robot's poses and positions over time was exported.

The extracted DBH estimations performed similarly to the way reported in other research studies of mobile mapping in forest. However beyond what has been reported in the literature, we found a relationship linking the support ratio to the accuracy of circle fit method. Furthermore, with a support ratio over 0.5, the quality of DBH estimates was much improved, and this topic deserves more attention. The extraction the positions of single trees was accurate too, which indicates that graph optimisation is successful and it opens the door for precise forest navigation.

Overall, the study uncovered many potential research opportunities for using SLAM in the forest environment. The complexity of forest structures and environment together with climate conditions pose challenges for implementing SLAM. Thus, further studies should focus on the need for more robust techniques of SLAM to deal with these aspects.

Acknowledgements

The authors wish to thank Arne Drømtorp for help building the robot platform, David Landry for his support in the robot programming and Bruce Talbot for help with the field work arrangements. The project received funding from the Norwegian Research Council (225329/E40).

References

Arita, Y., di Maria, E., Gallone, R., Capodieci, L., Morita, M., Okubo, K., Giannoccaro, N.I., Shige-Eda, M., and Nishida, T., 2016. Development of a Mobile Robot Platform for 3d Measurement of Forest Environments. <http://lab.cntl.kyutech.ac.jp/nishida/paper/2016/ThBT3.5.pdf>. (Accessed: 2016-12-15).

Astrup, R., Ducey, M.J., Granhus, A., Ritter, T., von Lüpke, N., 2014. Approaches for estimating stand-level volume using terrestrial laser scanning in a single-scan mode. Can. J. For. Res. 44 (6), 666–676.

Bailey, T., Nieto, J., Guivant, J., Stevens, M., Nebot, E., 2006. Consistency of the ekf-slam algorithm. In: 2006 IEEE/RSJ International Conference on Intelligent Robots and Systems. IEEE, pp. 3562–3568.

Béland, M., Widlowski, J.-L., Fournier, R.A., Côté, J.-F., Verstraete, M.M., 2011. Estimating leaf area distribution in savanna trees from terrestrial lidar measurements. Agric. For. Meteorol. 151 (9), 1252–1266.

Brunner, A., Gizachew, B., 2014. Rapid detection of stand density, tree positions, and tree diameter with a 2d terrestrial laser scanner. Eur. J. For. Res. 133 (5), 819–831.

Dellaert, F., 2012. Factor Graphs and gtsam: A Hands-on Introduction. <https://smartech.gatech.edu/handle/1853/45226> (Accessed: 2016-12-01).

Ducey, M.J., Astrup, R., Seifert, S., Pretzsch, H., Larson, B.C., Coates, K.D., 2013. Comparison of forest attributes derived from two terrestrial lidar systems. Photogramm. Eng. Rem. Sens. 79 (3), 245–257.

Ester, M., Kriegel, H.-P., Sander, J., Xu, X., 1996. A density-based algorithm for discovering clusters in large spatial databases with noise. In: Proceedings of 2nd International Conference on Knowledge Discovery and Data Mining, vol. 96. AAAI Press, pp. 226–231.

Forsman, M., Holmgren, J., Olofsson, K., 2016. Tree stem diameter estimation from mobile laser scanning using line-wise intensity-based clustering. Forests 7 (9), 206.

Grisetti, G., Kummerle, R., Stachniss, C., Burgard, W., 2010. A tutorial on graph-based slam. IEEE Intell. Transport. Syst. Mag. 2 (4), 31–43.

Grisetti, G., Stachniss, C., Burgard, W., 2009. Nonlinear constraint network optimization for efficient map learning. IEEE Trans. Intell. Transport. Syst. 10 (3), 428–439.

Hauglin, M., Gobakken, T., Astrup, R., Ene, L., Næsset, E., 2014. Estimating single-tree crown biomass of norway spruce by airborne laser scanning: a comparison of methods with and without the use of terrestrial laser scanning to obtain the ground reference data. Forests 5 (3), 384–403.

Hellström, T., Johansson, T., Ringdahl, O., 2006. Development of an autonomous forest machine for path tracking. In: Field and Service Robotics. Springer, pp. 603–614.

Holopainen, M., Vastaranta, M., Hyyppä, J., 2014. Outlook for the next generations precision forestry in finland. Forests 5 (7), 1682–1694.

Jaakkola, A., Hyyppä, J., Kukko, A., Yu, X., Kaartinen, H., Lehtomäki, M., Lin, Y., 2010. A low-cost multi-sensoral mobile mapping system and its feasibility for tree measurements. ISPRS J. Photogramm. Rem. Sens. 65 (6), 514–522.

Kazhdan, M., Hoppe, H., 2013. Screened poisson surface reconstruction. ACM Trans. Graphics (TOG) 32 (3), 29.

Liang, X., Kankare, V., Hyyppä, J., Wang, Y., Kukko, A., Haggrén, H., Yu, X., Kaartinen, H., Jaakkola, A., Guan, F., et al., 2016. Terrestrial laser scanning in forest inventories. ISPRS J. Photogramm. Rem. Sens. 115, 63–77.

Liu, J., Liang, X., Hyyppä, J., Yu, X., Lehtomäki, M., Pyörälä, J., Zhu, L., Wang, Y., Chen, R., 2017. Automated matching of multiple terrestrial laser scans for stem mapping without the use of artificial references. Int. J. Appl. Earth Obs. Geoinf. 56, 13–23.

Miettinen, M., Ohman, M., Visala, A., Forsman, P., 2007. Simultaneous localization and mapping for forest harvesters. In: Proceedings 2007 IEEE International Conference on Robotics and Automation. IEEE, pp. 517–522.

Mur-Artal, R., Montiel, J., Tardós, J.D., 2015. Orb-slam: a versatile and accurate monocular slam system. IEEE Trans. Robot. 31 (5), 1147–1163.

Næsset, E., Gobakken, T., Holmgren, J., Hyyppä, H., Hyyppä, J., Maltamo, M., Nilsson, M., Olsson, H., Persson, Å., Söderman, U., 2004. Laser scanning of forest resources: the nordic experience. Scand. J. For. Res. 19 (6), 482–499.

Nelson, E., 2016. B(erkeley) l(ocalization) a(nd) m(apping). <https://github.com/erik-nelson/blam> (Accessed: 2016-09-30).

Nistér, D., Naroditsky, O., Bergen, J., 2006. Visual odometry for ground vehicle applications. J. Field Robot. 23 (1), 3–20.

Olsoy, P.J., Forbey, J.S., Rachlow, J.L., Nobler, J.D., Glenn, N.F., Shipley, L.A., 2014. Fearscapes: mapping functional properties of cover for prey with terrestrial lidar. Bioscience 1, 74–80.

Pierzchała, M., Talbot, B., Astrup, R., 2014. Estimating soil displacement from timber extraction trails in steep terrain: application of an unmanned aircraft for 3d modelling. Forests 5 (6), 1212.

Pratt, V., 1987. Direct least-squares fitting of algebraic surfaces. In: ACM SIGGRAPH Computer Graphics, vol. 21. ACM, pp. 145–152.

Puliti, S., Ørka, H.O., Gobakken, T., Næsset, E., 2015. Inventory of small forest areas using an unmanned aerial system. Rem. Sens. 7 (8), 9632–9654.

Quigley, M., Conley, K., Gerkey, B., Faust, J., Foote, T., Leibs, J., Wheeler, R., Ng, A.Y., 2009. Ros: an open-source robot operating system. In: ICRA Workshop on Open Source Software, vol. 3, Kobe, Japan, p. 5.

Rahlf, J., Breidenbach, J., Solberg, S., Astrup, R., 2015. Forest parameter prediction using an image-based point cloud: a comparison of semi-itc with aba. Forests 6 (11), 4059–4071.

Ringdahl, O., Hellström, T., Wästerlund, I., Lindroos, O., 2012. Estimating wheel slip for a forest machine using rtk-dgps. J. Terrramech. 49 (5), 271–279.

Ringdahl, O., Hohnloser, P., Hellström, T., Holmgren, J., Lindroos, O., 2013. Enhanced algorithms for estimating tree trunk diameter using 2d laser scanner. Rem. Sens. 5 (10), 4839.

Rönnholm, P., Liang, X., Kukko, A., Jaakkola, A., Hyyppä, J., 2016. Quality analysis and correction of mobile backpack laser scanning data. ISPRS Ann. Photogramm., Rem. Sens. Spatial Inform. Sci., pp. 41–47.

Schnabel, R., Wahl, R., Klein, R., 2007. Efficient ransac for point-cloud shape detection. In: Computer Graphics Forum, vol. 26. Wiley Online Library, pp. 214–226.

Siciliano, B., Khatib, O., 2008. Springer Handbook of Robotics. Springer Science & Business Media.

Smith, A., Astrup, R., Raumonen, P., Liski, J., Krooks, A., Kaasalainen, S., Åkerblom, M., Kaasalainen, M., 2014. Tree root system characterization and volume estimation by terrestrial laser scanning and quantitative structure modeling. Forests 5 (12), 3274–3294.

Tang, J., Chen, Y., Kukko, A., Kaartinen, H., Jaakkola, A., Khoramshahi, E., Hakala, T., Hyyppä, J., Holopainen, M., Hyyppä, H., 2015. Slam-aided stem mapping for forest inventory with small-footprint mobile lidar. Forests 6 (12), 4588–4606.

Thies, M., Spiecker, H., 2004. Evaluation and future prospects of terrestrial laser scanning for standardized forest inventories. Forest 2 (2.2), 1.

Triebel, R., Pfaff, P., Burgard, W., 2006. Multi-level surface maps for outdoor terrain mapping and loop closing. In: 2006 IEEE/RSJ International Conference on Intelligent Robots and Systems, pp. 2276–2282.

Turner, D., Lucieer, A., Watson, C., 2012. An automated technique for generating georectified mosaics from ultra-high resolution unmanned aerial vehicle (uav) imagery, based on structure from motion (sfm) point clouds. Rem. Sens. 4 (5), 1392.

Vosselman, G., Maas, H.-G., 2010. Airborne and Terrestrial Laser Scanning. Whittles Publishing.

White, J.C., Wulder, M.A., Vastaranta, M., Coops, N.C., Pitt, D., Woods, M., 2013. The utility of image-based point clouds for forest inventory: a comparison with airborne laser scanning. Forests 4 (3), 518–536.

Wurm, K.M., Hornung, A., Bennewitz, M., Stachniss, C., Burgard, W., 2010. Octomap: A probabilistic, flexible, and compact 3d map representation for robotic systems. In: Proceedings of the ICRA 2010 Workshop on Best practice in 3D Perception and Modeling for Mobile Manipulation, vol. 2.